Journal of the Optical Society of America B
OPTICAL PHYSICS

Shaping of nanosecond pulses in ytterbium fiber lasers by synchronous sine-wave pump modulation

S. V. Smirnov,[1] B. N. Nyushkov,[1,2,*] A. V. Ivanenko,[1] D. B. Kolker,[1,2] and S. M. Kobtsev[1]

[1]Novosibirsk State University, Novosibirsk 630090, Russia
[2]Novosibirsk State Technical University, Novosibirsk 630073, Russia
*Corresponding author: b.nyushkov@nsu.ru

Received 16 July 2020; revised 22 August 2020; accepted 23 August 2020; posted 24 August 2020 (Doc. ID 402985); published 23 September 2020

In this work, we discovered the possibility of greatly relaxing requirements to the speed and dynamic range of pump power variation and, thus, of reducing synchronous pumping of ytterbium (Yb)-based fiber lasers to a very simple pump modulation yielding a mode-locked pulsed output. We show that even slow (microsecond-scale) low-index (≤0.5) sine-wave synchronous modulation of the pump power can result in shaping of a regular train of nanosecond laser pulses. It is revealed that the energy-conservative process of laser pulse shortening against the pump modulation period can take place in the quasi–two-level laser active medium owing to mistiming-induced gain discrimination of the temporal laser pulse profile. Thus, nanosecond pulses with energy up to 50 nJ were obtained in our experimental all-fiber Yb-based laser configuration. Our theoretical modeling reveals routes to much stronger pulse shortening through tunable pump modulation parameters. This discovery allows the establishment of more reliable and easy-to-implement high-efficiency alternatives to other types of high-energy ultralong mode-locked fiber lasers.

https://doi.org/10.1364/JOSAB.402985

1. INTRODUCTION

The development of reliable all-fiber laser sources of stable high-energy short and ultrashort pulses is a topical field of laser physics. As an alternative to the rather volatile *Q*-switched operation of fiber laser sources [1,2], innovative mode-locking methods and techniques significantly advance this field. Among them is all-normal-dispersion high-energy mode-locked operation [3,4] boosted by cavity lengthening toward kHz-scale pulse repetition rates [5–10]. Although the initial idea of such pulse energy enhancement seemed to be quite promising, the practical constraints turned out to be substantial. The main practical drawback of ultralong mode-locked lasers arose from their tendency to produce outputs with high noise figures: large interpulse intervals cause strong amplified spontaneous emission (ASE) contribution [8,11]. Polarization instability, overdriving of the mode-locker, and parasitic stimulated Raman scattering (SRS) are among other inherent factors which can drastically affect such lasers [8,12,13] and often lead to generation of irregular pulse bunches, noise-like [8] or so-called double-scale pulses [14,15]. To prevent those unwanted effects, various sophisticated cavity configurations, which allow the proper management of ASE, polarization, intracavity power, and SRS [8,10,11,16], were developed along with some improved methods of passive mode-locking [17–20] for high-energy pulsed lasing in ultralong fiber lasers. However, those approaches are usually associated with significant experimental complexity and cost, and more importantly, require careful adjustment of some intracavity parameters to sustain a desirable low-noise single-pulse mode-locked operation (for instance, traditional mode-locking based on nonlinear polarization evolution requires fine polarization control).

Thus, in the case of ultralong fiber lasers, it may be interesting to consider an alternative solution for obtaining high-energy pulsed lasing, namely, active mode-locking. Although comparison of noise and coherence properties of ultralong lasers with passive and active mode-locking deserves a separate study, the latter approach might feature a simpler implementation and more reliable operation. However, its conventional realization by means of an intracavity modulator (such as a Mach–Zehnder intensity modulator) cannot provide desirable high-energy performance due to the significant insertion loss and limited modulation capability in the case of relatively large spectral bandwidths of the laser radiation [21]. On the other hand, there are modulator-free approaches to active mode-locking.

They are associated with synchronous pumping. Synchronous pumping is an energy-efficient method for active mode-locking, typically used in bulk, dye, semiconductor, and Raman fiber lasers [22–27]. However, in diode-pumped fiber lasers with stimulated emission [such as Yb- or erbium (Er)-fiber lasers], the potentialities of this method were not yet fully explored. Shaping of short or ultrashort pulses by this method implies proper gain dynamics (i.e., variation of population inversion of laser energy levels). It is induced both by pump modulation and repeatable interaction of the generated light pulse with laser energy levels. Conventional diode pump sources have rather small modulation bandwidth, typically limited to tens of kHz. Thus, one might expect relatively slow gain dynamics leading to microsecond-scale pulse profiling. But actual laser gain dynamics could be rather more complicated. It can be governed by cross-timing of seed and pump modulation within limits of the energy levels scheme involved for amplification as shown in Ref. [28]. Although the long-life-time active medium stores pump energy integrally, the instantaneous gain can feature small but fast variation induced by circulating laser pulses. Therefore, in this work, we explore the possibility of relaxing requirements for the speed and dynamic range of pump power modulation when implementing synchronous pumping at 0.98 μm in Yb-based fiber lasers.

Our work stems from the idea that slight mistiming of synchronous pump modulation can induce gain discrimination of the temporal laser pulse profile in a laser active medium described by the effectively two-level model [29], thereby leading to laser pulse shortening against the pump modulation period. Such a pulse-profiling mechanism should feature relatively high energy efficiency because it is not based on energy dissipation unlike saturable absorbers or intensity modulators used in traditional mode-locking methods. It also differs substantially from conventional gain switching [30,31] driven by on–off switching of the pump. In our method, the weakly modulated pump power is always kept much above the lasing threshold. Therefore, the steady-state lasing is sustained continuously, and the relative amplitude of induced gain oscillations is found to be very small (<1%). Moreover, the gain oscillation period is quite strictly (with 0.01% tolerance) determined by the cavity round-trip time because of the synchronous nature of the demonstrated steady-state pulsed operation. This feature, along with the mistiming-induced laser pulse shortening, makes the demonstrated lasing regime also very different from the so-called "bias-pumped gain-switched" operation which was proposed in the theoretical work [32] mainly as a possible solution to the problem of relaxation oscillations and pulse shape control in gain-switched lasers. Therefore, we associate the discovered lasing regime with active mode-locking sustained by very weak quasi-synchronous gain modulation. Such a lasing regime with inherent laser pulse shortening has been explored and explained for the first time, to the best of our knowledge. In what follows, we corroborate our concept experimentally and theoretically. We demonstrate, for the first time, energy-efficient shaping of nanosecond pulses in a mode-locker-free Yb-fiber laser whose mode-locked-like operation was driven by slow (microsecond-scale) sine-wave pump modulation. Useful features of such a lasing regime are discussed along with the potential of the method for other types of active fibers.

2. EXPERIMENTAL

Layout of our primary experimental setup is presented in Fig. 1. The laser cavity has a ring-linear all-fiber configuration. It sustains counter-propagation of pump and lasing waves in the active ring part of the cavity. The counter-propagation scheme ensures that the output laser radiation is not mixed with residual pumping radiation. To prevent the contribution of nonlinear polarization evolution to laser pulse shaping, we composed the cavity of polarization-maintaining (PM) elements. The active cavity ring contains all essential elements: 0.55 m long Yb-doped active fiber (nLIGHT LIEKKI Yb700-6/125-PM), a 980/1064-nm wavelength-division multiplexor (WDM), a 5% output coupler, a 2 nm passband spectral filter centered at ∼1064 nm, and an optical circulator (CIR). The latter ensures unidirectional lasing in the cavity ring, and connects it with the linear arm which serves solely for the effective cavity lengthening by PM fiber and reduction of the fundamental pulse repetition rate. This arm is terminated by a circulator-based loop mirror [33]. Pumping radiation from two PM-fiber-coupled laser diodes (LDs) is combined by a polarization beam combiner (PBC). The total pump power injected into the Yb-fiber reached 1.1 W at most.

Pump power was manipulated through modulation inputs of the LD current drivers. Their modulation bandwidth is limited to ∼0.74 MHz (as determined at −3 dB level). The achievable pump modulation depth dramatically decreases with further increase of modulation frequency at their modulation inputs. These relatively slow LD current drivers formed the electronic bottleneck in the pump modulation system. The modulating signal was synthesized by a radiofrequency arbitrary waveform generator (RF AWG—Rigol DG4162) capable of operating at much higher frequencies. However, fast and deep arbitrary modulation of heavy current in high-power pumping LDs is a generally known technical issue that is more complicated for more powerful LDs. Thus, the explored shaping of relatively short laser pulses by relatively slow and weak pump modulation definitely possesses a practical value.

First, continuous-wave (CW) laser performance was explored: we measured output-pump power characteristics and optical spectra when applying direct-current (DC) voltage to the modulation inputs of the LD current drivers. The results are presented in Figs. 2(a) and 2(c). They indicate that the lasing threshold is achieved at a pump power of 0.13 W, laser output saturates at pump powers over 0.75 W, and optical spectrum has 0.43 nm width and is centered at 1064.9 nm. The spectral

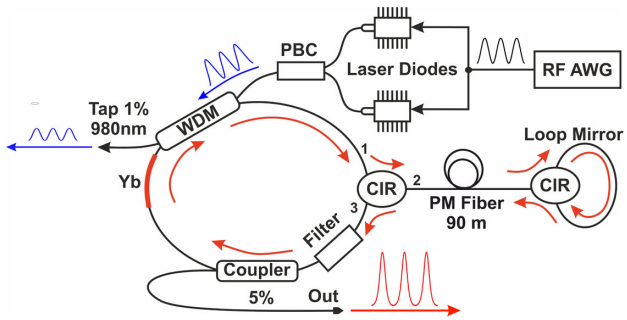

Fig. 1. Layout of the all-PM Yb-fiber laser with synchronously-modulated pumping.

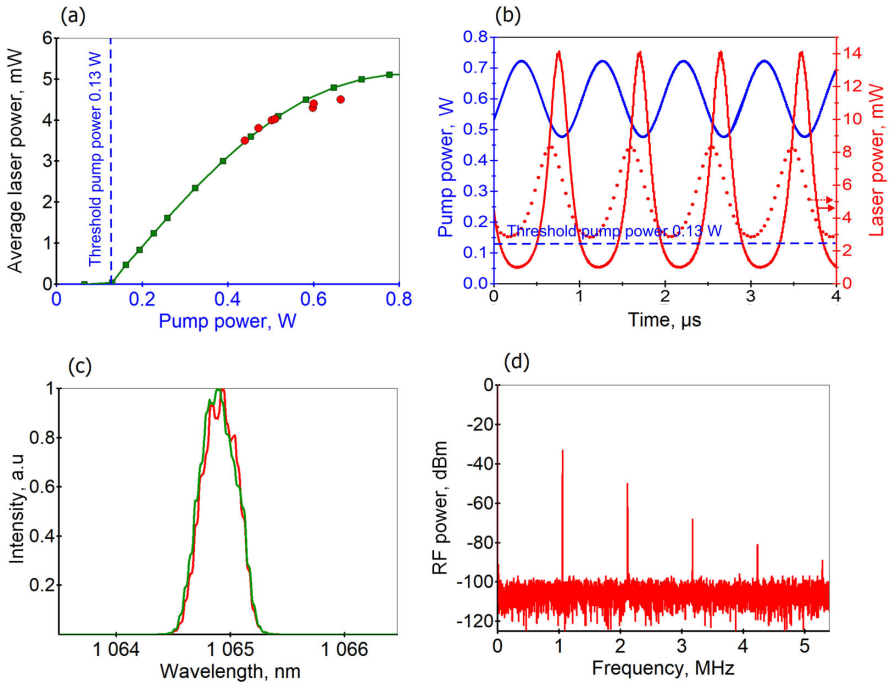

Fig. 2. Laser characteristics under continuous-wave (CW) and synchronously-modulated (SM) pumping: (a) average laser power versus average pump power in the CW regime (green trace) and in the SM regimes producing pulses with the contrast ≥90% (red circles); (b) oscillograms of the SM pump signal (solid blue trace), resulting laser pulse train (solid red trace) driven at the fundamental repetition rate of ∼1.058 MHz, and transient pulse-to-CW output obtained upon excessive detuning of the repetition rate by ∼100 Hz (dotted red trace); (c) optical spectra of the laser radiation acquired under CW pumping (green trace) and SM pumping (red trace); (d) radiofrequency spectrum of the laser pulse train generated at the fundamental repetition rate (resolution 1 kHz).

characteristics were not noticeably affected by pump power variation.

To switch the laser to the pulsed operation, we applied a sine-wave modulating signal to the LD current drivers. The modulation frequency was set to match the fundamental pulse repetition rate (∼1.058 MHz) determined by the cavity round-trip time. When approaching this rate, the laser output power begins oscillating synchronously with the modulating signal [as indicated by the dotted red trace in Fig. 2(b)]. Generally, that oscillation was rather similar to low-index sine-wave modulation than to the pulse shaping. However, it was revealed that the oscillating laser output converted into a regular train of relatively narrow pulses upon careful adjustment of the modulation frequency as indicated by the solid red trace in Fig. 2(b). This time trace represents the obtained laser pulse train with a contrast of 93% and pulse duration of 240 ns. This duration is four times shorter than the modulation period [pump power modulation is indicated by the blue trace in Fig. 2(b)]. The effect was pronounced only when the average value of the modulated pump power was high enough (over 0.44 W) and its modulation index exceeded 0.15 (being defined as a ratio of pump modulation amplitude to pump average value). These parameters are found to be limits for shaping laser pulses with contrast above 90%.

The radiofrequency (RF) spectrum of this pulse train [Fig. 2(d)] manifests comparatively high signal-to-noise ratio (70 dB at the fundamental pulse repetition frequency), thereby indicating proper quality of mode-locking. Since the generated pulses have a smooth nearly-Gaussian shape, their RF spectrum features a monotonic decrease of discrete spectral intensities with frequency (in accordance with the Fourier transform of the temporal pulse profile). Thus, there is no large-scale wavy pattern in intensity distribution across the obtained frequency comb as opposed to mode-locked generation of square-shaped [34], *h*-shaped [35], and other complicated waveforms [36,37]. The measured optical spectrum does not manifest noticeable broadening against the CW lasing as seen in Fig. 2(c). The pump modulation index was just 0.21 in the described case, while the average value of pump power was 0.6 W. The average laser output power amounted to 4.4 mW (giving net pulse energy of 3.4 nJ). We examined several combinations of the allowable pump modulation settings which enabled laser pulse contrast over 90%. To this end, we alternated the average pump power from 0.44 W to 0.66 W and the modulation index from 0.15 to 0.34. The measured average output powers of pulsed lasing at those average pump powers fit quite well (with limited measurement accuracy) the CW laser power characteristic as shown in Fig. 2(a). It testifies to the energy-conservative nature of the pulse shaping.

It was empirically revealed that the laser pulse contrast rises both with the modulation index and pump power average value. However, the limited modulation bandwidth of the LD current drivers did not allow us to surpass the previously indicated modulation indexes and average pump power values at the modulation frequency of 1.058 MHz. Therefore, it was necessary to reduce the fundamental pulse repetition rate further in order to avoid strong integration of the modulation signal by

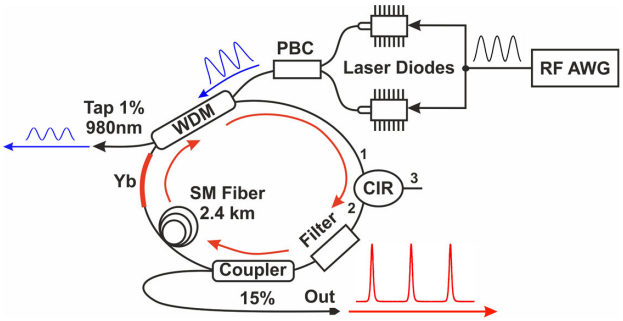

Fig. 3. Layout of the ultralong Yb-fiber laser with synchronously-modulated pumping.

the LD current drivers and, thus, to enable higher modulation indexes. To this effect, we elongated the laser cavity by inserting an available 2.4 km long single-mode fiber. It was inserted into the cavity ring, and the cavity linear arm was eliminated for loss reduction (as shown in Fig. 3). The 5% output coupler was replaced with a 15% one. This modified cavity configuration allowed the fundamental pulse repetition rate to be as low as ~88.78 kHz and, thus, to fit the available modulation bandwidth.

The measured output characteristics of such ultralong Yb-fiber laser with synchronously-modulated pumping are presented in Fig. 4. The laser output-pump power characteristics are given in Fig. 4(a), while the optical spectrum is depicted in Fig. 4(c). One may notice slightly increased power efficiency which is due to enhanced output coupling. Oscillogram of the laser pulse train [red trace in Fig. 4(b)] obtained upon fine adjustment of the modulation frequency manifests relatively high contrast (98%) and strong compression of laser pulses down to 750 ns. This duration is 15 times shorter than the pump modulation period [pump power modulation is represented by the blue time trace in Fig. 4(b)]. Average laser output power amounted to ~5.8 mW (giving net pulse energy of ~50 nJ). RF spectrum of this pulse train features high signal-to-noise ratio (72 dB at the fundamental pulse repetition frequency), thereby indicating proper quality of mode-locking [Fig. 4(d)]. Nonmonotonic decrease of discrete spectral intensities with frequency indicates that the pulse shape has appreciably diverged from the regular Gaussian one. Nevertheless, this pulse shaping was more effective (in terms of duration and contrast) than the primary laser configuration. This is due to higher modulation index (~0.5) at a relatively high average value of the pump power (0.61 W). A reduction in the modulation index led to degradation of pulse shaping as illustrated by the dotted time traces in Fig. 4(b) for a modulation index of 0.18 at an average pump power of 0.78 W. We examined several combinations of the allowable pump modulation settings that enabled laser pulse contrast over 95%.

To that end, we alternated the average pump power from 0.51 W to 0.72 W and the modulation index from 0.28 to 0.81. The measured average output powers of pulsed lasing at those average pump powers fit (with limited measurement accuracy) the CW laser power characteristic quite well, as shown in Fig. 4(a). It testifies to the energy-conservative nature of the pulse shaping in the modified laser cavity configuration.

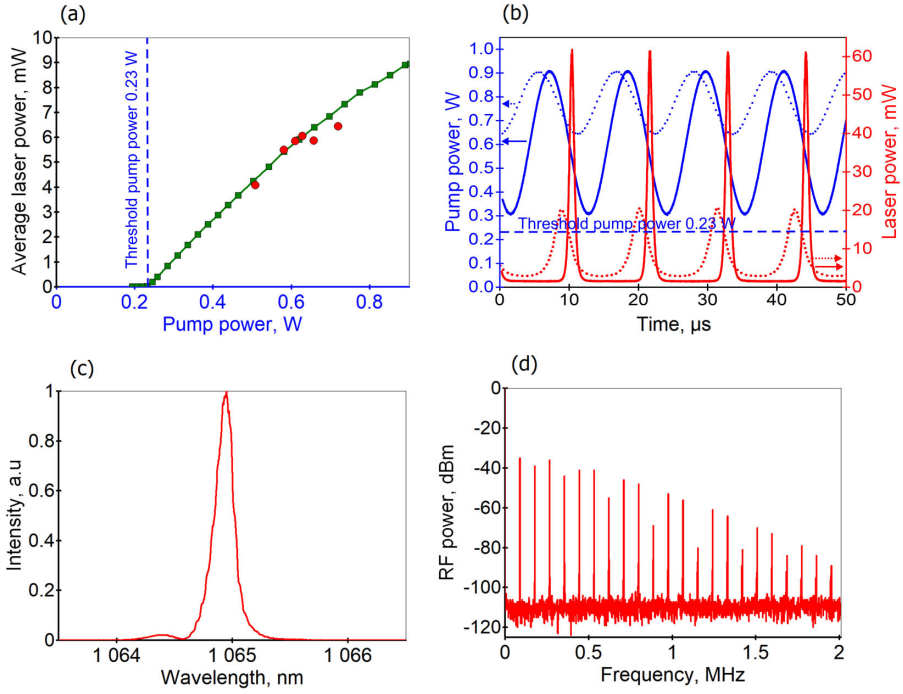

Fig. 4. Laser characteristics under continuous-wave (CW) and synchronously-modulated (SM) pumping: (a) average laser power versus average pump power in the CW regime (green trace) and in the SM regimes producing pulses with the contrast ≥95% (red circles); (b) oscillograms of the SM pump signal (solid blue trace), resulting in a laser pulse train (solid red trace) driven at the fundamental repetition rate of ~88.78 kHz, and transient pulse-to-CW output (dotted red trace) obtained upon lowering of the pump modulation index (as indicated by dotted blue trace); (c) optical spectra of laser radiation acquired under SM pumping; (d) radiofrequency spectrum of the laser pulse train generated at the fundamental repetition rate (resolution 0.2 kHz).

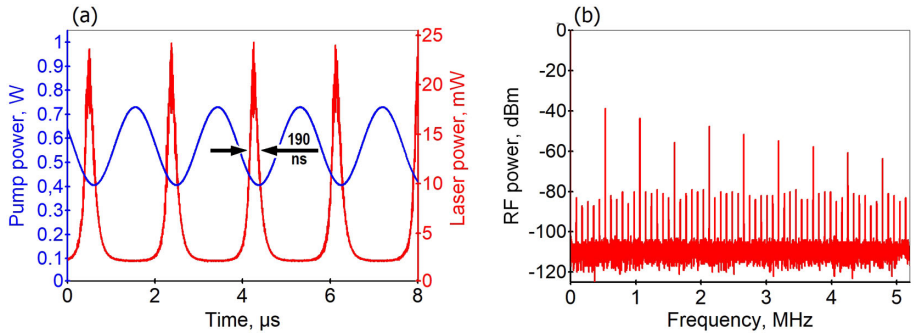

Fig. 5. Laser characteristics under synchronously-modulated (SM) pumping and operation at the sixth harmonic of the fundamental pulse repetition rate: (a) oscillograms of the SM pump signal (blue trace), and a resulting laser pulse train (red trace) driven at the harmonic repetition rate of ~531.5 kHz; (b) radiofrequency spectrum of the laser pulse train generated at the harmonic repetition rate (resolution 0.2 kHz).

Finally, we also explored the possibility of harmonic mode-locking by synchronous sine-wave pump modulation. To this effect, the modulation frequency was set at nearly 532 kHz to match the sixth harmonic of the fundamental repetition rate. Further, fine adjustment of the modulation parameters allowed laser generation of a nanosecond pulse train represented by the red time trace in Fig. 5(a). The pulses had a contrast of 92% and a duration of 190 ns. This duration was almost 10 times shorter than the pump modulation period [indicated by blue trace in Fig. 5(a)].

Slight lowering of the pulse contrast as against the operation at the fundamental repetition rate was due to decay of the pump modulation index. At the harmonic repetition rate, the pump modulation index was as low as 0.29, while the average value of pump power was 0.57 W. Nevertheless, the RF spectrum [Fig. 5(b)] of the obtained pulse train featured good signal-to-noise ratio (65 dB in the vicinity of the actual pulse repetition frequency) and relatively strong suppression of supermodes (which appear between RF components corresponding to the actual pulse repetition frequency). Supermode suppression ratio was ~40 dB around the actual pulse repetition frequency, which is comparable with analogous characteristics of other types of harmonic mode-locked fiber lasers [35,38]. These features testify to the proper quality of harmonic mode-locking. Average laser output power amounted to ~4.7 mW (giving net pulse energy of ~5.1 nJ).

Thus, we have experimentally discovered the energy-conservative effect of nanosecond pulse shaping in Yb-fiber lasers driven by microsecond-scale synchronous sine-wave pump modulation. Relatively low peak power and narrow spectral bandwidth of laser pulses suggest that it is hardly possible to associate the observed pulse shaping with the earlier known mechanisms of laser pulse shaping which involve optical nonlinearity and dispersion of fiber laser cavities [3,4]. It was empirically revealed that the crucial role in the observed pulse shaping is played by small mistiming (of the order of 0.01%) between the pump modulation period and the cavity round-trip time of slightly delayed laser pulses. This mistiming leads to gain discrimination of the temporal laser pulse profile, thereby making the pulse shorter. The amount of this mistiming is easily controlled by adjustment of the pump modulation frequency at the RF AWG. The relative mistiming can be treated as the relative mismatch between the modulation frequency and an effective frequency determined by the cavity round-trip time. For instance, at a pulse repetition rate of ~1 MHz, the crucial (for pulse shortening) frequency mismatch is ~100 Hz. There is no technical hurdle to control the modulation frequency even with a much better accuracy. Of course, the cavity round-trip time can also drift due to changes in the fiber optical length caused by thermal expansion. However, for a quartz fiber, 0.01% change in its optical length requires a temperature excursion in excess of 20°C. Thus, the proposed laser can reliably sustain a pulsed operation in conventional laboratory conditions for a long time. We had been observing its persistent pulsed operation for an entire work day.

It is important to note that steady-state pulse shaping of this type was possible only under certain conditions determined by such modulation parameters as modulation index, average pump power value, and pulse repetition rate mistiming. In the following section, we validate and study numerically the previously mentioned empirical supposition by using an earlier established theoretical framework [29] to describe gain dynamics in our Yb-fiber lasers.

3. THEORETICAL

In order to simulate pulse train generation, we used a transport equation with gain and loss terms:

$$\frac{n}{c}\frac{\partial P_s}{\partial t}+\frac{\partial P_s}{\partial z}+\alpha P+\alpha_c P\delta(z-z_c)+g P\delta(z-z_a)=0, \quad \textbf{(1)}$$

where t and z denote time and space coordinates along the fiber, c is velocity of light in free space, $n=1.45$ is effective refractive index of optical fiber, $\alpha=0.369\ \mathrm{km}^{-1}$ denotes effectively distributed intracavity optical losses (which corresponds to ~3.8 dB in total), $\alpha_c=0.85$ stands for lumped losses at the output coupler with 15% output, and g is the optical amplification coefficient. Since the optical amplifier length is much less than total cavity length, we assumed amplification to be lumped, $g(z)\propto\delta(z-z_a)$; z_c and z_a are z-coordinates of the output coupler and optical amplifier, respectively. In order to integrate Eq. (1) numerically, we used uniform mesh with $N=2^{12}=4096$ points and step size $h\sim 0.5$ m. We checked also that the results are reproduced on meshes with a different number of points ranging from 2^{10} up to 2^{13}. For numerical integration of Eq. (1) over time

t, we used a temporal mesh with step $hn/c \sim 2.4$ ns, which makes the integration procedure extremely simple. At each integration step, one has to shift power $P_j \equiv P(t_j)$ by one mesh step h: $P_{j+1} \leftarrow P_j \cdot \exp(-\alpha h)$, where $P_N \equiv P_0$ is for ring cavity. At two specific cavity points $z = z_c$ and $z = z_a$, one should also apply lump losses and gain by multiplying the intracavity power by corresponding factors. As an initial condition, we used CW noise with constant power as low as of 10^{-15} W.

In order to simulate optical amplification inside an Yb-doped fiber, we numerically solve Eq. (5) from Ref. [29]. Since we aimed for qualitative analysis of pulse generation, we used in our simulations parameters of active fibers given in Ref. [29]. For the sake of simplicity, we assumed the concentration of excited ions N_2 to be constant along the amplifier, which leads to exponential power distributions $P_p(z)$ and $P_s(z)$. In order to integrate numerically the ordinary differential equation for N_2 (see Eq. (5) in Ref. [29]), we used mean (i.e., z-averaged) values of these exponential functions $P_p(z)$ and $P_s(z)$.

Figure 6 shows simulation results obtained with sine-wave pump modulation at frequencies $f_p = (6 + 2.4 \times 10^{-4}) f_0$ (a) and $f_p = (6 - 2.4 \times 10^{-4}) f_0$ (b), where $f_0 = c/(nL)$ is the fundamental pulse repetition frequency determined by the cavity length L. It can be seen in Fig. 6(a) that relatively short pulses (nearly eight times shorter than the pump modulation period) appear in simulations when pump modulation frequency is slightly higher than the sixth harmonic of f_0. In contrast, in the case $f_p < 6 f_0$, no pulse shortening takes place, and the lasing power oscillogram looks similar to the pump power oscillogram [as seen in Fig. 6(b)]. Note that both observations agree well with the experiment (except the lower level of inter-pulse background which may be explained by the absence of spontaneous emission in the model). It is also worth noting that the relative amplitude of the induced gain oscillations is found to be very small (<1%) in steady-state pulsed operations, and the average gain is unaffected by a crucial (for pulse shaping) change in pump modulation frequency as seen in the upper graphs of Fig. 6. Now let us try to understand such pulse shaping qualitatively.

Let us consider sine-wave modulated pumping at a frequency f_p slightly higher than the mth harmonic of the fundamental pulse repetition frequency f_0 (e.g., in simulations discussed previously $m = 6$). Let us assume that the laser oscillates in a stationary regime, i.e., its power output is a periodic function of time: $P_{\text{out}}(t + T) = P_{\text{out}}(t)$, where t is an arbitrary time moment, and T is a period. Obviously, the pulse repetition rate for such stationary lasing must be equal to the pump modulation frequency ($1/T = f_p$) since driven oscillations always occur at driving force frequency. In the considered case of slightly increased pump modulation frequency, at the end of each cavity round-trip (after passing through the whole passive part of the cavity), the laser pulse comes to the amplifying fiber a little bit later than if this pulse were constantly propagating with its average velocity $L \cdot f_p/\text{m}$ that corresponds to round-trip time $T_{\text{RT}} = m/f_p$. If we define $P(\tau)$ as the power at amplifier output in a frame of references running with the average velocity $L \cdot f_p/\text{m}$ of the pulse, after passing through the passive part of the cavity, the power can be written as $kP(\tau - \delta t)$, where coefficient $k < 1$ stands for integral power losses at a round-trip, and δt is a small time delay related to the frequency mismatch $\delta t = (mf_0)^{-1} - f_p^{-1} \approx \delta f/f^2$, where $\delta f = f_p - m f_0$ is the frequency mismatch and $f \approx m f_0 \approx f_p$. Note that for the relatively long pulses that are considered here, one can neglect chromatic dispersion and nonlinear effects; that is why the pulse shape $P(\tau)$ remains intact as the pulse is traveling along the cavity. In order to restore the power $P(\tau)$ at the amplifier exit at the next round-trip and thus to sustain stationary lasing with repetition rate f_p, the amplifier should introduce the time-dependent amplification coefficient $g(\tau) = P(\tau)/[kP(\tau - \delta t)]$. Since the time delay δt is very small, we can use Taylor series expansion and approximate this as

$$g(\tau) = k^{-1} \cdot \left[1 + \delta t \cdot P'(\tau)/P(\tau)\right], \tag{2}$$

where $P'(\tau)$ stands for derivative $\mathrm{d}P(\tau)/\mathrm{d}\tau$. At the leading edge of the pulse, $P' > 0$ and thus, this part of the pulse experiences some excess amplification (i.e., amplification is greater than inverse losses, $g > k^{-1}$), whereas at the trailing edge,

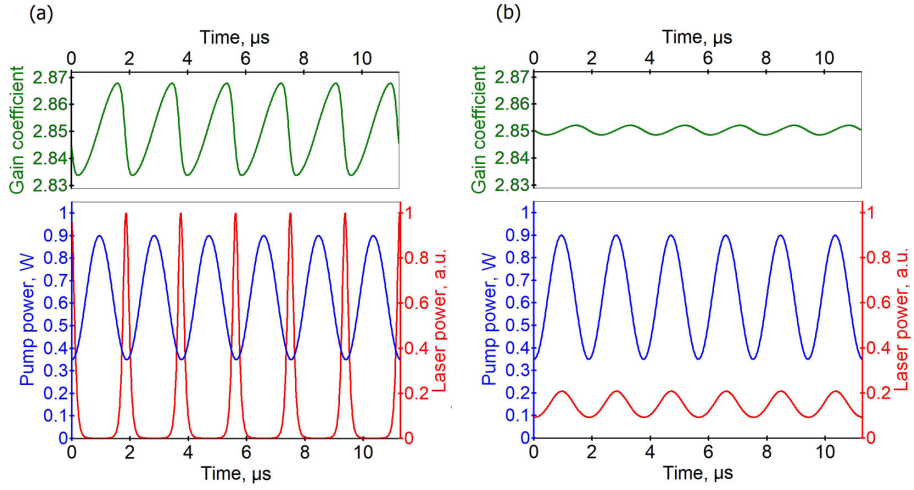

Fig. 6. Simulation results. Upper graphs: time traces of gain coefficient variation; lower graphs: corresponding time traces of pump (blue) and lasing (red) power variations. Results are presented for (a) positively and (b) negatively detuned pump modulation frequencies $f_p = (6 + 2.4 \times 10^{-4}) f_0$ and $f_p = (6 - 2.4 \times 10^{-4}) f_0$ respectively, where $f_0 = c/(nL)$ is the fundamental pulse repetition frequency determined by the cavity length L.

$P' < 0$ and amplification is lower than average ($g < k^{-1}$). This mechanism allows the amplifier to slightly "accelerate" the "retarded" pulse and to achieve a stationary lasing under small frequency mismatch $\delta f \ll f$. The reason for time-dependent gain is quite clear: as could be seen from Fig. 6(a), the amplifier accumulates pump energy during the most part of the modulation period $T = f_p^{-1}$, thus providing relatively high amplification for the leading edge of the pulse. As the leading edge of the pulse takes away a portion of the accumulated energy, the amplification coefficient becomes lower for the trailing edge of the pulse.

It is also quite evident now why no short pulse generation occurs in the opposite case $f_p < m f_0$: the amplification coefficient cannot be higher for the trailing edge (as against the leading edge) of a short pulse since the amplifier has no time to reaccumulate pump energy. Thus, in the case $f_p < m f_0$, the laser generates relatively long pulses whose trailing edge is located right after the maximum of pump power [see Fig. 6(b)]. Such timing maximizes the amplification available for the trailing edge. In contrast, when $f_p > m f_0$ [see Fig. 6(a)] the generated pulse train is shifted by a half period with respect to pump modulation that allows the pulse leading edge to have maximum amplification.

Now let us assume that the laser generates relatively short pulses. With the use of Eq. (2), let us try to anticipate how we can get shorter pulses $P(\tau)$. We can roughly estimate $P'(\tau)/P(\tau)$ at the pulse edges as $\pm\tau_0^{-1}$, where τ_0 stands for the pulse duration. Amplification coefficient g in Eq. (2) varies in a certain range whose width $g_{\max} - g_{\min}$ depends on amplifier parameters (such as fiber length and ion concentration) as well as on average pump power, pump modulation frequency f_p, and on lasing regime. With the use of approximation $\delta t \approx \delta f / f^2$, we can derive from Eq. (2):

$$\tau_0 \approx \frac{2\delta f}{f^2 k \cdot (g_{\max} - g_{\min}).} \tag{3}$$

Thus, one could expect that shorter pulses may be generated at a low frequency mismatch δf and at a higher frequency f (the latter can be increased e.g., by switching to higher harmonics of the fundamental repetition rate.) It should be stressed, however, that the difference $g_{\max} - g_{\min}$ is inversely proportional to the pump modulation frequency f_p, and therefore, pulse duration τ_0 is actually proportional to f^{-1}. Note also that with lower modulation index, the laser tends to produce a higher CW background. This leads to a decrease of $g_{\max} - g_{\min}$ and, consequently, to the growth of pulse duration τ_0. Thus, greater pump modulation depth facilitates shorter pulse generation. These conclusions are corroborated by our preliminary results of numerical simulations and will be further investigated theoretically and experimentally in more detail. Finally, it should be noted that parameter area of the stationary pulsed regime becomes narrower for shorter pulse durations, so it may be challenging to find and sustain lasing regimes with much shorter pulses. This question also should be investigated in more detail in the future.

It is also worth noting that the revealed pulse-shaping effect is rather universal for Yb-fiber lasers with synchronously-modulated pumping; the effect is not specific for the considered lasers schemes. The numerical model involved in the previously mentioned qualitative analysis effectively reduces pumping features (such as core/cladding pumping, counter/copropagating pumping), thereby corroborating the possibility of such a pulsed operation in different configurations of Yb-fiber lasers with proper sets of modulation parameters. Moreover, we have checked in our numerical model that similar pulse shaping can be achieved even if the lifetime of the upper laser level is set to be 8 ms (i.e., to be as long as in Er-doped active fibers). Moderate adjustment of modulation parameters within the same limits (imposed by the previously mentioned pump source and laser configuration) has been sufficient to that end. The latter feature suggests that the proposed method may be applicable to Er-based fiber lasers as well. Comprehensive study of such applicability will be conducted in our future studies.

4. SUMMARY

The energy-conservative effect of nanosecond pulse shaping in Yb-fiber lasers driven by microsecond-scale synchronous sine-wave pump modulation was discovered and studied both experimentally and theoretically for the first time. The crucial role in the revealed pulse-shaping effect is played by small mistiming (on the order of 0.01%) of the pump modulation period from the cavity round-trip time of slightly delayed laser pulses. This mistiming leads to gain discrimination of the temporal laser pulse profile, thereby making the pulse shorter. Thus, it is possible to shape a regular train of nanosecond laser pulses by even slow (microsecond-scale) low-index ($\leq$0.5) sine-wave synchronous modulation of the pump power. This effect is pronounced in Yb-fiber lasers with different types of cavities and allows mode-locked lasing with high-pulse energy enhanced by kilometer-scale elongation of the laser cavity. Theoretical modeling predicts the possibility of much stronger pulse shortening (by more than one order of magnitude) provided that certain pump modulation parameters (higher modulation frequency with proper offset and higher modulation index) are sustained. The effect is expected to be pronounced also in other fiber-based lasers with stimulated emission, provided that kinetics of energy levels involved into the lasing are qualitatively similar to those of the Yb-fiber lasers. For instance, this may be the case for Er-fiber lasers pumped at 1480 nm. When pumped at this wavelength, an Er-fiber can be effectively described as a two-level active medium. The previous findings open the prospect for establishment of novel high-energy all-fiber mode-locked laser sources which may become more a reliable, energy-efficient, easy-to-implement alternative to other types of high-energy ultralong mode-locked fiber lasers. The demonstrated approach also contributes to the important field of new methods for all-electronic control over pulsed lasing regimes in different types of fiber lasers [39–42].

Funding. Russian Science Foundation (17-12-01281); Ministry of Science and Higher Education of the Russian Federation (FSUS-2020-0036).

Acknowledgment. B. N. Nyushkov, A. V. Ivanenko, and S. M. Kobtsev thank the Russian Science Foundation for their support of this experimental study in the frame of the project 17-12-01281. S. V. Smirnov thanks the Ministry of

Science and Higher Education of the Russian Federation for their support of his numerical study in the frame of the project FSUS-2020-0036.

Disclosures. The authors declare no conflicts of interest.

REFERENCES

1. W. Shi, M. A. Leigh, J. Zong, Z. Yao, and D. T. Nguyen, "High-power all-fiber based narrow-linewidth single-mode fiber laser pulses in the C-band and frequency conversion to THz generation," IEEE J. Sel. Top. Quantum Electron. **15**, 377–384 (2009).
2. Y. M. Chang, J. Lee, Y. M. Jhon, and J. H. Lee, "Active Q-switching in an erbium-doped fiber laser using an ultrafast silicon-based variable optical attenuator," Opt. Express **19**, 26911–26916 (2011).
3. F. W. Wise, A. Chong, and W. H. Renninger, "High-energy femtosecond fiber lasers based on pulse propagation at normal dispersion," Laser Photon. Rev. **2**, 58–73 (2008).
4. P. Grelu and N. Akhmediev, "Dissipative solitons for mode-locked lasers," Nat. Photonics **6**, 84–92 (2012).
5. S. Kobtsev, S. Kukarin, and Y. Fedotov, "Ultra-low repetition rate mode-locked fiber laser with high-energy pulses," Opt. Express **16**, 21936–21941 (2008).
6. X. Tian, M. Tang, P. P. Shum, Y. Gong, C. Lin, S. Fu, and T. Zhang, "High-energy laser pulse with a submegahertz repetition rate from a passively mode-locked fiber laser," Opt. Lett. **34**, 1432–1434 (2009).
7. E. J. R. Kelleher, J. C. Travers, E. P. Ippen, Z. Sun, A. C. Ferrari, S. V. Popov, and J. R. Taylor, "Generation and direct measurement of giant chirp in a passively mode-locked laser," Opt. Lett. **34**, 3526–3528 (2009).
8. B. N. Nyushkov, A. V. Ivanenko, S. M. Kobtsev, S. K. Turitsyn, C. Mou, L. Zhang, V. I. Denisov, and V. S. Pivtsov, "Gamma-shaped long-cavity normal-dispersion mode-locked Er-fiber laser for sub-nanosecond high-energy pulsed generation," Laser Phys. Lett. **9**, 59–67 (2012).
9. R. I. Woodward, E. J. R. Kelleher, T. H. Runcorn, S. Loranger, D. Popa, V. J. Wittwer, A. C. Ferrari, S. V. Popov, R. Kashyap, and J. R. Taylor, "Fiber grating compression of giant-chirped nanosecond pulses from an ultra-long nanotube mode-locked fiber laser," Opt. Lett. **40**, 387–390 (2015).
10. A. Ivanenko, S. Kobtsev, S. Smirnov, and A. Kemmer, "Mode-locked long fibre master oscillator with intra-cavity power management and pulse energy >12 μJ," Opt. Express **24**, 6650–6655 (2016).
11. Y. Senoo, N. Nishizawa, Y. Sakakibara, K. Sumimura, E. Itoga, H. Kataura, and K. Itoh, "Ultralow-repetition-rate, high-energy, polarization-maintaining, Er-doped, ultrashort-pulse fiber laser using single-wall-carbon-nanotube saturable absorber," Opt. Express **18**, 20673–20680 (2010).
12. C. Aguergaray, A. Runge, M. Erkintalo, and N. G. R. Broderick, "Raman-driven destabilization of mode-locked long cavity fiber lasers: fundamental limitations to energy scalability," Opt. Lett. **38**, 2644–2646 (2013).
13. A. E. Bednyakova, S. A. Babin, D. S. Kharenko, E. V. Podivilov, M. P. Fedoruk, V. L. Kalashnikov, and A. Apolonski, "Evolution of dissipative solitons in a fiber laser oscillator in the presence of strong Raman scattering," Opt. Express **21**, 20556–20564 (2013).
14. S. Kobtsev, S. Kukarin, S. Smirnov, S. Turitsyn, and A. Latkin, "Generation of double-scale femto/pico-second optical lumps in mode-locked fiber lasers," Opt. Express **17**, 20707–20713 (2009).
15. S. Smirnov, S. Kobtsev, S. Kukarin, and A. Ivanenko, "Three key regimes of single pulse generation per round trip of all-normal-dispersion fiber lasers mode-locked with nonlinear polarization rotation," Opt. Express **20**, 27447–27453 (2012).
16. D. S. Kharenko, V. A. Gonta, and S. A. Babin, "50 nJ 250 fs all-fibre Raman-free dissipative soliton oscillator," Laser Phys. Lett. **13**, 025107 (2016).
17. S. Smirnov, S. Kobtsev, A. Ivanenko, A. Kokhanovskiy, A. Kemmer, and M. Gervaziev, "Layout of NALM fiber laser with adjustable peak power of generated pulses," Opt. Lett. **42**, 1732–1735 (2017).
18. A. Kokhanovskiy, S. Kobtsev, A. Ivanenko, and S. Smirnov, "Properties of artificial saturable absorbers based on NALM with two pumped active fibres," Laser Phys. Lett. **15**, 125101 (2018).
19. S. Boscolo, C. Finot, I. Gukov, and S. K. Turitsyn, "Performance analysis of dual-pump nonlinear amplifying loop mirror mode-locked all-fibre laser," Laser Phys. Lett. **16**, 065105 (2019).
20. F. B. Braham, G. Semaan, A. Niang, A. Komarov, F. Bahloul, M. Salhi, K. Komarov, and F. Sanchez, "Wave-breaking-free passively mode-locked fiber laser using a hybrid regime of oscillation," Laser Phys. Lett. **15**, 095401 (2018).
21. N. A. Koliada, B. N. Nyushkov, A. V. Ivanenko, S. M. Kobtsev, P. Harper, S. K. Turitsyn, V. I. Denisov, and V. S. Pivtsov, "Generation of dissipative solitons in an actively mode-locked ultralong fibre laser," Quantum Electron **43**, 95–98 (2013).
22. J. C. AuYeung and A. R. Johnston, "Picosecond pulse generation from a synchronously pumped mode-locked semiconductor laser diode," Appl. Phys. Lett. **40**, 112–114 (1982).
23. D. S. Peter, P. Beaud, W. Hodel, and H. P. Weber, "Passive stabilization of a synchronously pumped mode-locked dye laser with the use of a modified outcoupling mirror," Opt. Lett. **16**, 405–407 (1991).
24. E. Granados, H. M. Pask, and D. J. Spence, "Synchronously pumped continuous-wave mode-locked yellow Raman laser at 559 nm," Opt. Express **17**, 569–574 (2009).
25. B. N. Nyushkov, S. M. Kobtsev, A. K. Komarov, K. P. Komarov, and A. K. Dmitriev, "SOA fiber laser mode-locked by gain modulation," J. Opt. Soc. Am. B **35**, 2582–2587 (2018).
26. S. Kobtsev, A. Ivanenko, A. Kokhanovskiy, and M. Gervaziev, "Raman-converted high-energy double-scale pulses at 1270 nm in P_2O_5-doped silica fiber," Opt. Express **26**, 29867–29872 (2018).
27. D. S. Kharenko, V. D. Efremov, E. A. Evmenova, and S. A. Babin, "Generation of Raman dissipative solitons near 1.3 microns in a phosphosilicate-fiber cavity," Opt. Express **26**, 15084–15089 (2018).
28. H. Tünnermann, J. Neumann, D. Kracht, and P. Weßels, "Gain dynamics and refractive index changes in fiber amplifiers: a frequency domain approach," Opt. Express **20**, 13539–13550 (2012).
29. S. K. Turitsyn, A. E. Bednyakova, M. P. Fedoruk, A. I. Latkin, A. A. Fotiadi, A. S. Kurkov, and E. Sholokhov, "Modeling of CW Yb-doped fiber lasers with highly nonlinear cavity dynamics," Opt. Express **19**, 8394–8405 (2011).
30. J. Yang, Y. Tang, and J. Xu, "Development and applications of gain-switched fiber lasers [Invited]," Photon. Res. **1**, 52–57 (2013).
31. Y. Hou, Q. Zhang, S. Qi, X. Feng, and P. Wang, "Monolithic all-fiber repetition-rate tunable gain-switched single-frequency Yb-doped fiber laser," Opt. Express **24**, 28761–28767 (2016).
32. F. Wang, "Stable pulse generation in a bias-pumped gain-switched fiber laser," J. Opt. Soc. Am. B **35**, 231–236 (2018).
33. S. M. Kobtsev, S. V. Kukarin, and Y. S. Fedotov, "Wide-spectrally-tunable CW and femtosecond linear fiber lasers with ultrabroadband loop mirrors based on fiber circulators," Laser Phys. **20**, 347–350 (2010).
34. J. Zhao, D. Ouyang, Z. Zheng, M. Liu, X. Ren, C. Li, S. Ruan, and W. Xie, "100 W dissipative soliton resonances from a thulium-doped double-clad all-fiber-format MOPA system," Opt. Express **24**, 12072–12081 (2016).
35. J. Zhao, L. Li, L. Zhao, D. Tang, D. Shen, and L. Su, "Tunable and switchable harmonic h-shaped pulse generation in a 3.03 km ultralong mode-locked thulium-doped fiber laser," Photon. Res. **7**, 332–340 (2019).
36. B. N. Nyushkov, S. M. Kobtsev, A. V. Ivanenko, and S. V. Smirnov, "Programmable optical waveform generation in a mode-locked gain-modulated SOA-fiber laser," J. Opt. Soc. Am. B **36**, 3133–3138 (2019).
37. B. Nyushkov, A. Ivanenko, S. Smirnov, and S. Kobtsev, "Electronically controlled generation of laser pulse patterns in a synchronously pumped mode-locked semiconductor optical amplifier-fiber laser," Laser Phys. Lett. **16**, 115103 (2019).
38. C. Mou, R. Arif, A. Rozhin, and S. Turitsyn, "Passively harmonic mode locked erbium doped fiber soliton laser with carbon nanotubes based saturable absorber," Opt. Mater. Express **2**, 884–890 (2012).
39. Y. Gladush, A. A. Mkrtchyan, D. S. Kopylova, A. Ivanenko, B. Nyushkov, S. Kobtsev, A. Kokhanovskiy, A. Khegai, M. Melkumov, M. Burdanova, M. Staniforth, J. Lloyd-Hughes, and A. G. Nasibulin,

"Ionic liquid gated carbon nanotube saturable absorber for switchable pulse generation," Nano Lett. **19**, 5836–5843 (2019).
40. A. Kokhanovskiy, A. Ivanenko, S. Kobtsev, S. Smirnov, and S. Turitsyn, "Machine learning methods for control of fibre lasers with double gain nonlinear loop mirror," Sci. Rep. **9**, 2916 (2019).
41. B. Nyushkov, A. Ivanenko, S. Smirnov, O. Shtyrina, and S. Kobtsev, "Triggering of different pulsed regimes in fiber cavity laser by a waveguide electro-optic switch," Opt. Express **28**, 14922–14932 (2020).
42. W. Margulis, A. Das, J. P. von der Weid, and A. S. L. Gomes, "Hybrid electronically addressable random fiber laser," Opt. Express **28**, 23388–23396 (2020).